

Article

# Polyvinylpyrrolidone-Stabilized Iridium Nanoparticles Catalyzed the Transfer Hydrogenation of Nitrobenzene Using Formic Acid as the Source of Hydrogen

Xinrui Zhou and Meng Zhou \* 

Department of Natural Sciences, Lawrence Technological University, 21000 West Ten Mile Road, Southfield, MI 48075, USA; xzhousisi1020@gmail.com

\* Correspondence: mzhou@ltu.edu

Received: 7 November 2020; Accepted: 8 December 2020; Published: 10 December 2020



**Abstract:** Catalytic nitrobenzene reduction is crucial for the synthesis of 4,4-methylene diphenyl diisocyanate, which is used to produce polyurethane foams, thermoplastic elastomers, and adhesives. The stability and activity of nanoparticle catalysts are affected by surface ligands and stabilizers. We established the complete composition of  $7.0 \pm 1.1$  nm iridium oxide nanoparticles that were stabilized by polyvinylpyrrolidone (PVP[Ir]). PVP[Ir] and its surface stabilizers were characterized using elemental analysis (EA), high-resolution X-ray photoelectron spectroscopy (XPS), powder X-ray diffraction (PXRD), FT-IR, and UV-vis spectroscopy. Notably, PVP[Ir] contained  $33.8 \pm 0.4\%$  Ir. XPS binding energy analyses suggest that 7% of the Ir is Ir(0) and 93% is IrO<sub>2</sub>. Using formic acid as the source of hydrogen, PVP[Ir] catalyzed the selective hydrogenation of nitrobenzene to give aniline as the only product in 66% yield in 1 h at 160 °C in a high-pressure metal reactor. Less than 1% of the side products (azobenzene and azoxybenzene) were detected. In contrast, using alcohol as the hydrogen source led to a low yield and a poor selectivity for aniline.

**Keywords:** iridium oxide nanoparticles; transfer hydrogenation; nitrobenzene reduction; catalysis; formic acid; alcohol; characterizations of nanoparticles

## 1. Introduction

Aniline is made in the industry primarily by the catalytic hydrogenation of nitrobenzene [1]. The vast majority of aniline is used as the precursor to 4,4-methylene diphenyl diisocyanate (MDI) [1]. In 2008, the demand for pure and polymeric MDI in the United States was 1.61 million metric tons [2]. MDI is used to manufacture polyurethane foams, thermoplastic elastomers, and adhesives [1,3]. Aniline is also a versatile reagent in organic synthesis via the Sandmeyer reaction [4]. Aniline and glycerol can undergo a Skraup condensation–cyclization reaction to form quinoline with nitrobenzene as the hydrogen acceptor [1,4].

The conventional approach to convert nitrobenzene to aniline via catalytic hydrogenation using Pd/C and H<sub>2</sub> is a notable safety hazard [5,6]. Pd/C is a pyrophoric material that can spontaneously spark in air and ignite methanol or filter paper [5–7], and H<sub>2</sub> is explosive [8,9]. In addition, the catalyst loading of Pd/C is typically high: 5% or more in Pd [5,6]. H<sub>2</sub> is mostly produced from the energy-intensive catalytic steam reforming of methane at 700–850 °C [10]. Therefore, alternative approaches that are safe and sustainable are preferred.

Modern synthetic methods for the catalytic hydrogenation of nitrobenzene have reduced the risk of combustion and Pd loading. Palladium(II) acetate was used as a safe precursor to generate Pd/C in situ [11]. Pd nanoparticles (NPs) embedded in an organically modified silica support were

an active and safe catalyst [6]. Meanwhile, transfer hydrogenation [12–17] has been developed to replace H<sub>2</sub> with organic compounds that can be derived from various resources such as biomass, CO<sub>2</sub>, and fossil fuels. Recently, the transfer hydrogenation of nitrobenzene has been realized using Pd [18–21] or Co [22–25] NPs as the catalyst and formic acid or ammonium formate as the source of hydrogen. Similar reactions can also be achieved using various metal complexes as the catalyst [26,27]. Nevertheless, the transfer hydrogenation of nitrobenzene can be performed without a transition metal catalyst and with NaOH, albeit with a low selectivity for aniline [16,28].

The stability and activity of nanoparticle (NP) catalysts are affected by surface ligands and stabilizers [29–31]. Reactive intermediates can coordinate with the NP surface atoms. Therefore, the surface chemistry of ligand and stabilizers is crucial for the rational design of NP catalysts and elucidating the mechanisms. The characterization of these ligands and stabilizers remains a great challenge [29–31].

In this work, we characterized the surface ligands and stabilizers on Ir NPs stabilized by polyvinylpyrrolidone (PVP). The NP stability, reactivity, and catalysis were investigated for the transfer hydrogenation of acetophenone and nitrobenzene. Although Ir NPs are active for catalytic hydrogenation using H<sub>2</sub> [32–38], the transfer hydrogenation of nitrobenzene was rarely studied [13].

## 2. Results and Discussion

We reproduced the literature synthesis of PVP-stabilized metallic Ir NPs (**PVP[Ir]**) using IrCl<sub>3</sub>·3H<sub>2</sub>O in the presence of PVP in an aqueous alcohol solvent under N<sub>2</sub> at 110 °C [39,40]. The alcohol is the reducing agent that converts Ir(III) to Ir(0). The synthesis in methanol [39] was used for the 7 ± 1.1 nm NPs with a high surface area and a narrow size distribution. The powder X-ray diffraction (PXRD), UV-vis, and FT-IR spectra of **PVP[Ir]** corroborated the original report [39]. A broad, amorphous reflection was observed in the PXRD analysis. No crystalline Ir reflections were detected, [41] which is consistent with amorphous NPs. A strong UV-vis absorption near 200 nm was assigned to the n-to-π\* transition [42] of the γ-lactam moiety in PVP. The lack of an absorption at 400 nm is consistent with the complete conversion of the starting material (IrCl<sub>3</sub>·3H<sub>2</sub>O). The strong lactam C=O stretch at 1630 cm<sup>-1</sup> was observed in the FT-IR analysis (Figure S1 in Supplementary Materials). **PVP[Ir]** powder was stable against aggregation for 3 months and can be readily redispersed in water, methanol, ethanol, and 2-propanol. Details of the experiments are described in the Supplementary Materials.

To establish the complete composition of **PVP[Ir]**, we performed elemental analysis (EA) and high-resolution X-ray photoelectron spectroscopy (XPS) analysis. Ir (33.8 ± 0.4%), C (21.59 ± 1.23%), H (3.97 ± 0.41%), and N (4.29 ± 0.26%) were detected by EA. These elements were attributed to the NP core and PVP stabilizer, which accounted for 63.66 ± 2.32% of the total mass. The C-to-N ratio of 5.9:1.0 in **PVP[Ir]** matched the 6:1 ratio in PVP. The H-to-N ratio of 12.9:1.0 is 43% higher than the 9:1 ratio in PVP. The excess hydrogen could be due to water, hydroxide ions, and surface hydride [29].

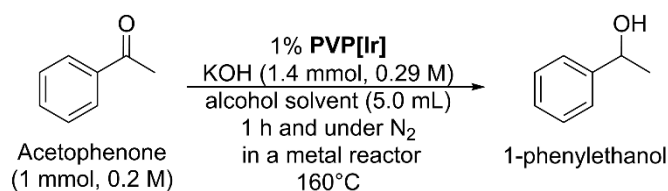
The other 36.34% of the mass was attributed to Na, O, and Cl, which were detected in an XPS survey spectrum. Sodium and chloride originated from NaOH and IrCl<sub>3</sub>·3H<sub>2</sub>O, which were used in the synthesis of **PVP[Ir]**. Chloride ions likely existed as Derjaguin–Landau–Verwey–Overbeek (DLVO) stabilizers [29,30] on the NPs with sodium as the counterions. No significant (<5%) NaCl crystalline phase was detected in the PXRD analysis of **PVP[Ir]**, which is consistent with the absence of a separate crystalline NaCl phase as an impurity. However, the presence of amorphous NaCl and NaOH impurities cannot be ruled out. Oxygen can come from PVP, water, air, or NaOH. Hydroxide ions can act as the surface ligands on Pt NPs [29,43]. The XPS analysis was performed using gold as the reference, which was sputtered on the sample, with an Au 4f<sub>7/2</sub> peak [29] at 84.0 eV.

High-resolution XPS binding energy analysis was performed on the Ir 4f<sub>7/2</sub> and 4f<sub>5/2</sub> binding energies of freshly made **PVP[Ir]** (Figure S2 in Supplementary Materials). Ir(0) in 7% and IrO<sub>2</sub> in 93% were detected. The binding energies at 60.76 and 63.74 eV were attributed to Ir metal, where the corresponding binding energies are 60.8 ± 0.2 and 63.8 eV [41]. The binding energies at 61.96 and 64.94 eV are consistent with IrO<sub>2</sub> (61.9 and 64.9 eV) [41]. Ir<sub>2</sub>O<sub>3</sub> (62.45 and 65.43 eV) [13] and IrCl<sub>3</sub>

(62.5 and 65.5 eV) [41] were not observed. Together with the lack of the  $\text{IrCl}_3$  absorption (400 nm) in the UV-vis analysis of **PVP[Ir]**, the presence of  $\text{IrCl}_3$  impurity is ruled out. The XPS results suggest that **PVP[Ir]** consists of partially reduced  $\text{IrO}_2$  NPs that were stabilized by PVP. The XPS spectra are available in the Supplementary Materials.

Methanol is a sustainable source of hydrogen that can be obtained from the  $\text{CO}_2$  reduction, biomass fermentation, and syngas ( $\text{H}_2$  and  $\text{CO}$ ) [15,44]. Methanol can serve as a hydrogen donor for the catalytic hydrogenation of aldehyde, [45] imine [15], and nitroarene [26,46] using transition-metal complexes or  $\text{Pd-Fe/Al}_2\text{O}_3$  [47]. Therefore, we studied the reactivity of **PVP[Ir]** toward methanol: **PVP[Ir]** was heated in a solution of  $\text{KOH}$  in methanol solution at  $160^\circ\text{C}$  for 1 h. At the end of the reaction, a carbonyl stretch at  $1875\text{ cm}^{-1}$  was detected by the FT-IR analysis (Figure S3 in Supplementary Materials). No carbonyl stretch was observed in **PVP[Ir]** before the reaction with methanol (Figure S3 in Supplementary Materials), which ruled out the possibility that the metal carbonyl stretch was due to **PVP[Ir]**. **PVP[Ir]** was synthesized in methanol at a relatively low temperature of  $110^\circ\text{C}$ , instead of  $160^\circ\text{C}$  as in this reactivity study. This metal carbonyl is unlikely to originate from the Na, O, and Cl impurities in **PVP[Ir]**. This stretching frequency is consistent with a metal carbonyl ( $1750\text{--}2050\text{ cm}^{-1}$ ) [48] but inconsistent with an iridium(0) carbonyl. A terminal iridium(0) carbonyl [49] ( $2025\text{ cm}^{-1}$ ) and an  $\text{Ir}_4(\text{CO})_{12}$  cluster [50] ( $2029$  and  $2069\text{ cm}^{-1}$ ) can be ruled out. The iridium(0)  $\mu_2$ -bridging carbonyl ( $1750\text{ cm}^{-1}$ ) can also be ruled out [49]. Although stretching frequencies close to  $1875\text{ cm}^{-1}$  have been reported for  $\mu_2$ -bridging carbonyl ligands on functionalized tetrairidium carbonyl clusters ( $1800$  to  $1878\text{ cm}^{-1}$ ), [51,52] the  $1875\text{ cm}^{-1}$  stretch cannot be assigned to such clusters due to the lack of any terminal carbonyl stretch. Overall, the coordination environment of this metal carbonyl is unclear. Surface metal carbonyl can poison a catalyst, [15,44] but it can also act as a NP stabilizer without the poisoning effect [29].

**PVP[Ir]** was used as a catalyst for the base-promoted transfer hydrogenation of acetophenone, which was a model reaction to identify an active hydrogen donor [12,16]. The nitrobenzene transfer hydrogenation can be complicated by the formation of side products (azobenzene, azoxybenzene) and is unsuitable for this purpose [16,47]. In an alcohol solvent with  $\text{KOH}$ , acetophenone was reduced to 1-phenylethanol at  $160^\circ\text{C}$  in 1 h in the presence of 1% **PVP[Ir]** (Scheme 1 and Table S1 in Supplementary Materials). The reaction was performed in a high-pressure metal reactor and heated in an oven. This setup enabled the reaction to take place at a higher temperature than the normal boiling point of the solvent, thus shortening reaction time. The 1% catalyst loading was calculated using the mole of acetophenone and the mole of Ir, measured by EA, in 7.7 mg of **PVP[Ir]**.



**Scheme 1.** The transfer hydrogenation of acetophenone catalyzed by **PVP[Ir]** using alcohol as the source of hydrogen. The results and reaction conditions are described in Table S1 of Supplementary Materials.

With methanol as the source of hydrogen, no product formed, and unreacted acetophenone was recovered (entry 1 in Table S1). Using ethanol as the source of hydrogen but under otherwise identical conditions, 1-phenylethanol formed in 53% yield with **PVP[Ir]** and 19% yield without **PVP[Ir]** (entry 2). The product yield from the **PVP[Ir]**-catalyzed reaction is 34% higher than the one without. Using 2-propanol as the source of hydrogen, the reaction was highly efficient regardless of whether **PVP[Ir]** is present. Only quantitative product formation was observed (entry 3 in Table S1). Details of the experimental procedures are described in the Supplementary Materials. The product yields inversely correlated with the alcohol  $\alpha$ -C-H bond strength [53]. The most reactive alcohol was 2-propanol, consistent with the related studies [14–16,28].

Given the significant reactivity of alcohols as the hydrogen source in the **PVP[Ir]**-catalyzed transfer hydrogenation of acetophenone, we studied the selectivity in the catalytic transfer hydrogenation of nitrobenzene under similar reaction conditions (Table 1). Ethanol was ineffective as the source of hydrogen for the nitrobenzene reduction (entry 1 in Table 1). Aniline was formed with only 5.3% yield, which is calculated by dividing the mole of aniline by the mole of nitrobenzene starting material. The partially reduced products azobenzene and azoxybenzene were formed in 1% and 7.1% yields, respectively. The selectivity of aniline to azobenzene and azoxybenzene (the dimers) was 0.65 to 1, favoring the dimer formation. The unreacted starting material was detected in 7% recovery yield, which suggests that 93% of the nitrobenzene has been converted. Dark red precipitates were found at the end of the reaction but were filtered out before the NMR analysis. The mass balance, which is calculated by adding together the aniline yield, the unreacted starting material recovery yield, and two times the yield of the dimers (two equivalents of nitrobenzene for one equivalent of dimer), is only 29%. This low mass balance suggests that 71% of the nitrobenzene starting material was converted to products that were not detectable by the  $^1\text{H}\{^{13}\text{C}\}$  NMR analysis. The lost 71% of the nitrobenzene starting material is attributed to the dark red precipitates that were filtered out before the NMR analysis. The precipitates could contain phenazine, a product from coupling nitrobenzene and aniline under basic conditions. [1] When 2-propanol was used as the source of hydrogen and under otherwise identical conditions (entry 2), the aniline yield increased drastically to 31%, and a reversal of selectivity occurred to favor aniline formation. A selectivity of 1.4:1 was observed. The unreacted starting material was recovered in 5% yield, and the mass balance was 84%. Dark red precipitates were again observed. In entry 3, the aniline yield decreased to 18%, and the selectivity reversed to 0.66:1 in a control experiment in the absence of **PVP[Ir]** but under otherwise identical conditions to those in entry 2. The unreacted starting material was recovered in 12% yield, and the mass balance was 84% (entry 3). **PVP[Ir]** was likely responsible for the higher yield and selectivity in the catalyzed reaction (entry 2) than those from the uncatalyzed reaction (entry 3).

**Table 1.** **PVP[Ir]** in the catalytic transfer hydrogenation of nitrobenzene to aniline.

Entry	Solvent	Aniline Yield <sup>a</sup>	AZB Yield <sup>a</sup>	AZXB Yield <sup>a</sup>	Aniline to Dimer Selectivity	Recovered SM <sup>b</sup>	Mass Balance <sup>c</sup>
1	Ethanol	5.30%	1%	7.10%	0.65:1	7%	29%
2	2-propanol	31%	14%	10%	1.4:1	5%	84%
3 <sup>d</sup>	2-propanol	18%	4%	23%	0.66:1	12%	84%
4 <sup>e</sup>	Methanol formic acid	66%	<1%	<1%	>66:1	40%	106%
5 <sup>d,e,f</sup>	Methanol formic acid	<1%	<1%	1%	N/A	19 ± 1%	22%

Reaction conditions unless otherwise specified: Nitrobenzene in 1.2 mmol or 0.24 M, KOH in 1.43 mmol, an alcohol solvent in 5.0 mL, 160 °C, 1 h, under  $\text{N}_2$ , and with 1% catalyst loading (11  $\mu\text{mol}$ ), which is calculated by dividing the mole of Ir, obtained from elemental analysis, by the mole of nitrobenzene, 1.2 mmol. AZB and AZXB denote azobenzene and azoxybenzene, respectively. The dimer refers to azobenzene and azoxybenzene. N/A denotes not applicable. All percentages are % mole. <sup>a</sup> Yields are calculated based on the starting material, nitrobenzene in 1.2 mmol, using quantitative  $^1\text{H}\{^{13}\text{C}\}$  NMR analysis with *p*-xylene as an internal standard; <sup>b</sup> SM denotes starting material (nitrobenzene); <sup>c</sup> mass balance = % yield of aniline + 2 × % yield of the dimers + % recovery yield of nitrobenzene starting material; <sup>d</sup> control experiments without the Ir catalyst; <sup>e</sup> the solvent is composed of 5 mL methanol and 88%wt aqueous formic acid in 0.43 mL (12 mmol of formic acid, 2.2 M in the 5.43 mL combined solution); <sup>f</sup> repeated twice.

When a methanol solution of formic acid (2.2 M in methanol) was used as the source of hydrogen in entry 4, the **PVP[Ir]**-catalyzed reaction gave aniline in 66% yield at 160 °C in 1 h. No significant (<1%) side products (azobenzene and azoxybenzene) or dark red precipitates formed. Nitrobenzene

was recovered in 40% yield. The mass balance was 106%. The >100% mass balance is likely due to the  $\pm 10\%$  error in the quantitative proton NMR analysis. Without PVP[Ir] and under otherwise identical conditions to entry 4, nearly no product formed, and the starting material was recovered in  $19 \pm 1\%$  yield (entry 5). No carbonyl stretch at  $1875\text{ cm}^{-1}$  was detected by FT-IR in a reaction of PVP[Ir] and formic acid in methanol (Figure S4 in Supplementary Materials), in contrast to the reaction of PVP[Ir] and pure methanol. Both results of the FT-IR analyses are reproducible.

The high reactivity of formic acid cannot be rationalized in terms of its C-H bond strength (96.6 kcal/mol), which is higher than those of the  $\alpha$ -C-H bonds of ethanol (95.9 kcal/mol), 2-propanol (94.8 kcal/mol), and propanol (95.5 kcal/mol) [53]. Propanol is present in <2% in the reagent-grade 2-propanol.

In general, formic acid is an efficient hydrogen donor because its dehydrogenation is exothermic ( $\Delta H^\circ = -7.9\text{ kcal/mol}$ ) [27,54,55]. The dehydrogenation of formic acid to  $\text{CO}_2$  and  $\text{H}_2$  is more thermodynamically favorable than the decarbonylation to CO and  $\text{H}_2\text{O}$  ( $\Delta H^\circ = -3.0\text{ kcal/mol}$ ) [27,54]. The formation of surface metal carbonyl with CO is a catalyst deactivation pathway, which is undesirable [15,44]. Selective dehydrogenation of formic acid to  $\text{CO}_2$  and  $\text{H}_2$  has been realized using homogeneous (ruthenium phosphine complexes) and heterogeneous catalysts (Ir/C and Pd/C) [27]. The selectivity for the dehydrogenation using Ir/C or Pd/C was close to 99%. In this work (entry 4 in Table 1), methanol was used as a solvent for the transfer hydrogenation using formic acid. The 88% formic acid solution contained 12% water, which can enhance the reactivity of methanol as a hydrogen donor [47]. Methanol was used as a hydrogen donor for the Pd-catalyzed nitroarene reduction in the presence of water. Water may facilitate the conversion of formaldehyde, the initial product of methanol dehydrogenation, [55] to formic acid [47].

In contrast, the dehydrogenation of methanol, ethanol, and 2-propanol to the corresponding aldehydes is endothermic [55–58]. Primary alcohols can be dehydrogenated to form aldehydes, which can undergo decarbonylation to form CO [59,60]. Methanol, ethanol, 1- and 2-propanol can undergo decarbonylation on a Pd metal surface to give CO and hydrocarbon [59]. Nevertheless, the formation of surface metal carbonyl does not necessarily poison a catalyst [29]. Although water can promote the catalytic hydrogenation of acetophenone using 2-propanol as the source of hydrogen [61,62], it is beyond the scope of this work to determine whether water can also promote 2-propanol for the catalytic nitrobenzene reduction.

The pressure was monitored over time for the catalytic transfer hydrogenation with formic acid at  $160\text{ }^\circ\text{C}$  (entry 4 in Table 1). The reaction was carried out in a high-pressure metal reactor equipped with a pressure gauge on a gage block assembly (Parr Instrument Company, Moline, IL, USA). Heating was carried out in a silicone oil bath that can withstand temperature up to  $200\text{ }^\circ\text{C}$  (Sigma-Aldrich, St. Louis, MO, USA). The pressure gauge (Wika Instrument, Lawrenceville, GA, USA) has a detection limit of  $2\text{--}140\text{ kg/cm}^2$  ( $1\text{ kg/cm}^2 = 0.98\text{ bar}$ ). Since the pressure gauge can be damaged at elevated temperature, only the reaction vessel was fully submerged in the oil bath. As described in entry 1 in Table 2, the temperature of the oil bath decreased from  $160$  to  $135\text{ }^\circ\text{C}$  soon after submerging the reactor in the oil bath, which had been pre-heated to  $160\text{ }^\circ\text{C}$ . The pressure of the reaction was  $4 \pm 1\text{ kg/cm}^2$ . Fifteen minutes later (entry 4 in bold), the temperature and pressure rose to  $160\text{ }^\circ\text{C}$  and  $20 \pm 1\text{ kg/cm}^2$ . Another fifteen minutes later (entry 7 in bold), the pressure reached the maximum of  $24 \pm 1\text{ kg/cm}^2$  and remained at this value till the end of the reaction (entries 7 to 15). This pressure cannot be fully accounted for by the vapor pressure of methanol solvent, which is  $16\text{ bar}$  ( $17\text{ kg/cm}^2$ ) at  $160\text{ }^\circ\text{C}$  [63]. The additional pressure of  $7 \pm 1\text{ kg/cm}^2$  could be attributed to the gases generated from the decomposition of formic acid. The dehydrogenation of formic acid is exothermic and can be catalyzed by Ir/C or Pd/C [27,54,55]. Therefore, we cannot rule out the possibility that  $\text{H}_2$  and  $\text{CO}_2$  gases were generated in situ from formic acid in the catalytic hydrogenation of nitrobenzene, where  $\text{H}_2$  served as the source of hydrogen. Ruppert et al. reported the transfer hydrogenation of levulinic acid using formic acid as the source of hydrogen with a ruthenium nanoparticle catalyst.  $\text{H}_2$ , along with  $\text{CO}_2$ , CO, and  $\text{CH}_4$ , was generated in situ in this reaction [64].

**Table 2.** Pressure over time for the catalytic transfer hydrogenation of nitrobenzene with formic acid.

Entry	Time (Hour/Minute)	Pressure (kg/cm <sup>2</sup> )	Temperature (°C)
1	0:00	4	135
2	0:05	9	140
3	0:10	18	146
4	0:15	20	160
5	0:20	22	160
6	0:25	23	160
7	0:30	24	160
8	0:35	24	160
9	0:40	24	160
10	0:45	24	160
11	0:50	24	160
12	0:55	24	160
13	1:00	24	160
14	1:05	24	160
15	1:10	24	160

### 3. Conclusions

The  $7 \pm 1.1$  nm **PVP[Ir]** NPs were partially reduced iridium oxide NPs with a  $33.8 \pm 0.4\%$  Ir content. The XPS binding energy analysis suggests that 7% of the iridium is metallic, and 93% is IrO<sub>2</sub>. Using alcohol as the source of hydrogen, the **PVP[Ir]**-catalyzed transfer hydrogenation of nitrobenzene was inefficient and unselective. In contrast, formic acid was superior to dry alcohol as the hydrogen source for the **PVP[Ir]**-catalyzed nitrobenzene reduction. **PVP[Ir]** catalyzed the selective transfer hydrogenation of nitrobenzene to aniline in 66% yield using formic acid as the source of hydrogen. No significant side products (azobenzene and azoxybenzene) formed in this reaction.

**Supplementary Materials:** The following are available online at <http://www.mdpi.com/2624-8549/2/4/61/s1>, Figure S1: FT-IR spectrum of **PVP[Ir]**, Figure S2: Binding energy analysis on the Ir 4f<sub>7/2</sub> and 4f<sub>5/2</sub> peaks of **PVP[Ir]**, Figure S3: **PVP[Ir]** before (grey) and after (red) the decarbonylation of methanol, Figure S4: **PVP[Ir]** before (grey) and after (red) the reaction with formic acid in methanol, Table S1: The **PVP[Ir]**-catalyzed transfer hydrogenation of acetophenone to 1-phenylethanol.

**Author Contributions:** X.Z. and M.Z. conducted the experiments and analyzed the data. M.Z. wrote the article. All authors have read and agreed to the published version of the manuscript.

**Funding:** This research received no external funding.

**Acknowledgments:** We thank the Lawrence Technological University Seed Grant 2018 for supporting this work. Xinrui Zhou thanks the HHMI for a student researcher award in 2018. We thank Patrick McCurdy at the Colorado State University, Robert Crabtree at Yale University, and Dennis Anderson at Wayne State University for helpful discussions.

**Conflicts of Interest:** There are no conflicts to declare.

### References

1. Amini, B.; Lowenkron, S. Aniline and Its Derivatives. In *Kirk-Othmer Encyclopedia of Chemical Technology*; Ley, C., Ed.; John Wiley and Sons: Hoboken, NJ, USA, 2003; Volume 2, pp. 783–800.
2. USEPA. *Methylene Diphenyl Diisocyanate (MDI) and Related Compounds Action Plan*; USEPA: Washington, DC, USA, 2011.
3. Parod, R.J. Diphenylmethane Diisocyanate (MDI), 4,4'. In *Encyclopedia of Toxicology*; Wexler, P., Ed.; Academic Press: Oxford, UK, 2014; pp. 1–5.
4. Kurti, L.; Czako, B. *Strategic Applications of Named Reactions in Organic Synthesis*; Elsevier Academic Press: Burlington, NJ, USA, 2005.
5. Hammond, C.N.; Schatz, P.F.; Mohrig, J.R.; Davidson, T.A. Synthesis and Hydrogenation of Disubstituted Chalcones. A Guided-Inquiry Organic Chemistry Project. *J. Chem. Educ.* **2009**, *86*, 234–239. [[CrossRef](#)]

6. Ramirez Côté, C.; Ciriminna, R.; Pandarus, V.; Béland, F.; Pagliaro, M. Comparing the Pyrophoricity of Palladium Catalysts for Heterogeneous Hydrogenation. *Org. Process Res. Dev.* **2018**, *22*, 1852–1855. [[CrossRef](#)]
7. Moreno, T.; García-Serna, J.; Plucinski, P.; Sánchez-Montero, M.J.; Cocero, M.J. Direct Synthesis of H<sub>2</sub>O<sub>2</sub> in Methanol at Low Pressures Over Pd/C Catalyst: Semi-Continuous Process. *Appl. Catal. A* **2010**, *386*, 28–33. [[CrossRef](#)]
8. Mirza, N.R.; Degenkolbe, S.; Witt, W. Analysis of Hydrogen Incidents to Support Risk Assessment. *Int. J. Hydrog. Energy* **2011**, *36*, 12068–12077. [[CrossRef](#)]
9. Dorofeev, S.B.; Kochurko, A.S.; Efimenko, A.A.; Chaivanov, B.B. Evaluation of the Hydrogen Explosion Hazard. *Nucl. Eng. Des.* **1994**, *148*, 305–316. [[CrossRef](#)]
10. *IEA Energy Technology Essentials: Hydrogen Production & Distribution*; International Energy Agency: Paris, France, 2007.
11. Felpin, F.-X.; Fouquet, E. A Useful, Reliable and Safer Protocol for Hydrogenation and the Hydrogenolysis of O-Benzyl Groups: The In Situ Preparation of an Active Pd<sup>0</sup>/C Catalyst with Well-Defined Properties. *Chem. Eur. J.* **2010**, *16*, 12440–12445. [[CrossRef](#)]
12. Wang, D.; Astruc, D. The Golden Age of Transfer Hydrogenation. *Chem. Rev.* **2015**, *115*, 6621–6686. [[CrossRef](#)]
13. Hammond, C.; Schümperli, M.T.; Conrad, S.; Hermans, I. Hydrogen Transfer Processes Mediated by Supported Iridium Oxide Nanoparticles. *ChemCatChem* **2013**, *5*, 2983–2990. [[CrossRef](#)]
14. Hillier, A.C.; Lee, H.M.; Stevens, E.D.; Nolan, S.P. Cationic Iridium Complexes Bearing Imidazol-2-ylidene Ligands as Transfer Hydrogenation Catalysts. *Organometallics* **2001**, *20*, 4246–4252. [[CrossRef](#)]
15. Campos, J.S.; Sharninghausen, L.S.; Manas, M.G.; Crabtree, R.H. Methanol Dehydrogenation by Iridium N-Heterocyclic Carbene Complexes. *Inorg. Chem.* **2015**, *54*, 5079–5084. [[CrossRef](#)]
16. Wang, D.; Deraedt, C.; Ruiz, J.; Astruc, D. Sodium Hydroxide-Catalyzed Transfer Hydrogenation of Carbonyl Compounds and Nitroarenes Using Ethanol or Isopropanol as Both Solvent and Hydrogen Donor. *J. Mol. Catal. A Chem.* **2015**, *400*, 14–21. [[CrossRef](#)]
17. Sabater, S.; Mata, J.A.; Peris, E. Dual Catalysis with an Ir<sup>III</sup>–Au<sup>I</sup> Heterodimetallic Complex: Reduction of Nitroarenes by Transfer Hydrogenation using Primary Alcohols. *Chem. Eur. J.* **2012**, *18*, 6380–6385. [[CrossRef](#)]
18. Cheng, S.; Meng, X.; Shang, N.; Gao, S.; Feng, C.; Wang, C.; Wang, Z. Pd Supported on g-C<sub>3</sub>N<sub>4</sub> Nanosheets: Mott-Schottky Heterojunction Catalyst for Transfer Hydrogenation of Nitroarenes Using Formic Acid as Hydrogen Source. *New J. Chem.* **2018**, *42*, 1771–1778. [[CrossRef](#)]
19. Neeli, C.K.P.; Puthiaraj, P.; Lee, Y.-R.; Chung, Y.-M.; Baeck, S.-H.; Ahn, W.-S. Transfer Hydrogenation of Nitrobenzene to Aniline in Water Using Pd Nanoparticles Immobilized on Amine-Functionalized UiO-66. *Catal. Today* **2018**, *303*, 227–234. [[CrossRef](#)]
20. Tuteja, J.; Nishimura, S.; Ebitani, K. Base-free Chemoselective Transfer Hydrogenation of Nitroarenes to Anilines with Formic Acid as Hydrogen Source by a Reusable Heterogeneous Pd/ZrP Catalyst. *RSC Adv.* **2014**, *4*, 38241–38249. [[CrossRef](#)]
21. Zhang, L.; Liu, X.; Zhou, X.; Gao, S.; Shang, N.; Feng, C.; Wang, C. Ultrafine Pd Nanoparticles Anchored on Nitrogen-Doping Carbon for Boosting Catalytic Transfer Hydrogenation of Nitroarenes. *ACS Omega* **2018**, *3*, 10843–10850. [[CrossRef](#)]
22. Duan, Y.; Song, T.; Dong, X.; Yang, Y. Enhanced Catalytic Performance of Cobalt Nanoparticles Coated with a N,P-Codoped Carbon Shell Derived from Biomass for Transfer Hydrogenation of Functionalized Nitroarenes. *Green Chem.* **2018**, *20*, 2821–2828. [[CrossRef](#)]
23. Guo, H.; Gao, R.; Sun, M.; Guo, H.; Wang, B.; Chen, L. Cobalt Entrapped in N,S-Codoped Porous Carbon: Catalysts for Transfer Hydrogenation with Formic Acid. *ChemSusChem* **2019**, *12*, 487–494. [[CrossRef](#)]
24. Yuan, M.; Long, Y.; Yang, J.; Hu, X.; Xu, D.; Zhu, Y.; Dong, Z. Biomass Sucrose-Derived Cobalt@Nitrogen-Doped Carbon for Catalytic Transfer Hydrogenation of Nitroarenes with Formic Acid. *ChemSusChem* **2018**, *11*, 4156–4165. [[CrossRef](#)]
25. Zhang, Y.; Cao, P.; Zhang, H.-Y.; Yin, G.; Zhao, J. Cobalt Nanoparticles Anchoring on Nitrogen Doped Carbon with Excellent Performances for Transfer Hydrogenation of Nitrocompounds to Primary Amines and N-substituted Formamides with Formic Acid. *Catal. Commun.* **2019**, *129*, 105747. [[CrossRef](#)]

26. Wienhöfer, G.; Sorribes, I.; Boddien, A.; Westerhaus, F.; Junge, K.; Junge, H.; Llusar, R.; Beller, M. General and Selective Iron-Catalyzed Transfer Hydrogenation of Nitroarenes without Base. *J. Am. Chem. Soc.* **2011**, *133*, 12875–12879. [[CrossRef](#)] [[PubMed](#)]
27. Grasemann, M.; Laurenczy, G. Formic Acid as a Hydrogen Source—Recent Developments and Future Trends. *Energy Environ. Sci.* **2012**, *5*, 8171–8181. [[CrossRef](#)]
28. Polshettiwar, V.; Varma, R.S. Revisiting the Meerwein–Ponndorf–Verley Reduction: A Sustainable Protocol for Transfer Hydrogenation of Aldehydes and Ketones. *Green Chem.* **2009**, *11*, 1313–1316. [[CrossRef](#)]
29. Zhou, M. Characterizations of Surface Ligands and Stabilizers on Metallic Nanoparticles. In *Catalysis by Metal Complexes and Nanomaterials: Fundamentals and Applications*; American Chemical Society: Washington, DC, USA, 2019; Volume 1317, pp. 103–133.
30. Ott, L.S.; Finke, R.G. Transition-Metal Nanocluster Stabilization for Catalysis: A Critical Review of Ranking Methods and Putative Stabilizers. *Coord. Chem. Rev.* **2007**, *251*, 1075–1100. [[CrossRef](#)]
31. Martínez-Prieto, L.M.; Chaudret, B. Organometallic Ruthenium Nanoparticles: Synthesis, Surface Chemistry, and Insights into Ligand Coordination. *Acc. Chem. Res.* **2018**, *51*, 376–384. [[CrossRef](#)]
32. Campos, C.; Torres, C.; Oportus, M.; Pena, M.A.; Fierro, J.L.G.; Reyes, P. Hydrogenation of substituted aromatic nitrobenzenes over 1% 1.0 wt.% Ir/ZrO<sub>2</sub> catalyst: Effect of Meta Position and Catalytic Performance. *Catal. Today* **2013**, *213*, 93–100. [[CrossRef](#)]
33. Fan, G.-Y.; Zhang, L.; Fu, H.-Y.; Yuan, M.-L.; Li, R.-X.; Chen, H.; Li, X.-J. Hydrous Zirconia Supported Iridium Nanoparticles: An Excellent Catalyst for the Hydrogenation of Haloaromatic Nitro Compounds. *Catal. Commun.* **2010**, *11*, 451–455. [[CrossRef](#)]
34. Jiang, H.-Y.; Xu, J.; Sun, B. Selective Hydrogenation of Aromatic Compounds Using Modified Iridium Nanoparticles. *Appl. Organomet. Chem.* **2018**, *32*, e4260. [[CrossRef](#)]
35. Li, H.-B.; Liu, L.; Ma, X.-Y. Effective Hydrogenation of Haloaromatic Nitro Compounds Catalysed by Iridium Nanoparticles Deposited on Multiwall Carbon Nanotubes. *Synth. React. Inorg. Met. Org. Nano-Met. Chem.* **2016**, *46*, 1499–1505. [[CrossRef](#)]
36. Ma, L.; Wang, J.; Wang, H.; Zhang, Q.; Lu, C.; He, X.; Li, X. High Halogenated Nitrobenzene Hydrogenation Selectivity over Nano Ir and Pd Particles. *Chin. J. Chem. Eng.* **2017**, *25*, 306–312. [[CrossRef](#)]
37. Motoyama, Y.; Taguchi, M.; Desmira, N.; Yoon, S.-H.; Mochida, I.; Nagashima, H. Chemoselective Hydrogenation of Functionalized Nitroarenes and Imines by Using Carbon Nanofiber-Supported Iridium Nanoparticles. *Chem. Asian J.* **2014**, *9*, 71–74. [[CrossRef](#)] [[PubMed](#)]
38. Tamura, M.; Kenichi, K.; Satsuma, A.; Shimizu, K.-I. Volcano-Curves for Dehydrogenation of 2-Propanol and Hydrogenation of Nitrobenzene by SiO<sub>2</sub>-Supported Metal Nanoparticles Catalysts as Described in Terms of a d-Band Model. *ACS Catal.* **2012**, *2*, 1904–1909. [[CrossRef](#)]
39. Goel, A.; Bhatt, R. Synthesis and Characterization of Nanoscale Colloidal Iridium Metal Clusters by Chemical Reduction Method Using Monohydric and Dihydric Alcohols. *Int. J. Chem. Appl.* **2012**, *4*, 111–121.
40. Bonet, F.; Delmas, V.; Grugeon, S.; Herrera Urbina, R.; Silvert, P.Y.; Tekaiia-Elhsissen, K. Synthesis of Monodisperse Au, Pt, Pd, Ru and Ir Nanoparticles in Ethylene Glycol. *Nanostruct. Mater.* **1999**, *11*, 1277–1284. [[CrossRef](#)]
41. Freakley, S.J.; Ruiz-Esquius, J.; Morgan, D.J. The X-ray Photoelectron Spectra of Ir, IrO<sub>2</sub> and IrCl<sub>3</sub> Revisited. *Surf. Interface Anal.* **2017**, *49*, 794–799. [[CrossRef](#)]
42. Zaman, A.C.; Kaya, C. Determination of Quantity of Materials in Suspensions and in Electrophoretic Coatings by UV-Visible Absorption Spectroscopy. *J. Electrochem. Soc.* **2015**, *162*, D3109–D3111. [[CrossRef](#)]
43. Schrader, I.; Warneke, J.; Neumann, S.; Grotheer, S.; Swane, A.A.; Kirkensgaard, J.J.K.; Arenz, M.; Kunz, S. Surface Chemistry of “Unprotected” Nanoparticles: A Spectroscopic Investigation on Colloidal Particles. *J. Phys. Chem. C* **2015**, *119*, 17655–17661. [[CrossRef](#)]
44. Palo, D.R.; Dagle, R.A.; Holladay, J.D. Methanol Steam Reforming for Hydrogen Production. *Chem. Rev.* **2007**, *107*, 3992–4021. [[CrossRef](#)]
45. Aboo, A.H.; Bennett, E.L.; Deeprose, M.; Robertson, C.M.; Iggo, J.A.; Xiao, J. Methanol as Hydrogen Source: Transfer Hydrogenation of Aromatic Aldehydes with a Rhodacycle. *Chem. Commun.* **2018**, *54*, 11805–11808. [[CrossRef](#)]
46. Reed-Berendt, B.G.; Mast, N.; Morrill, L.C. Manganese-Catalyzed One-Pot Conversion of Nitroarenes into N-Methylarylamines Using Methanol. *Eur. J. Org. Chem.* **2020**, *2020*, 1136–1140. [[CrossRef](#)]

47. Xiang, Y.; Li, X.; Lu, C.; Ma, L.; Zhang, Q. Water-Improved Heterogeneous Transfer Hydrogenation Using Methanol as Hydrogen Donor over Pd-Based Catalyst. *Appl. Catal. A* **2010**, *375*, 289–294. [[CrossRef](#)]
48. Conley, R.T. *Infrared Spectroscopy*, 2nd ed.; Allyn and Bacon: Boston, MA, USA, 1972.
49. Korányi, T.I.; Mihály, J.; Pfeifer, É.; Németh, C.; Yuzhakova, T.; Mink, J. Infrared Emission and Theoretical Study of Carbon Monoxide Adsorbed on Alumina-Supported Rh, Ir, and Pt Catalysts. *J. Phys. Chem. A* **2006**, *110*, 1817–1823. [[CrossRef](#)] [[PubMed](#)]
50. Shido, T.; Okazaki, T.; Ichikawa, M. EXAFS/FT-IR Characterization of Tetra-Iridium Carbonyl Clusters Bound to Tris-(Hydroxymethyl)Phosphine Grafted Silica Surface Catalytically Active for Propene Oxidation to Acetone. *J. Mol. Catal. A Chem.* **1997**, *120*, 33–45. [[CrossRef](#)]
51. Zhang, S.; Foyle, S.D.; Okrut, A.; Solovyov, A.; Katz, A.; Gates, B.C.; Dixon, D.A. Role of N-Heterocyclic Carbenes as Ligands in Iridium Carbonyl Clusters. *J. Phys. Chem. A* **2017**, *121*, 5029–5044. [[CrossRef](#)] [[PubMed](#)]
52. Gelin, P.; Naccache, C.; Taarit, Y.B. Coordination Chemistry of Rhodium and Iridium in Constrained Zeolite Cavities: Methanol Carbonylation. *Pure Appl. Chem.* **1988**, *60*, 1315–1320. [[CrossRef](#)]
53. Luo, Y.R. *Comprehensive Handbook of Chemical Bond Energies*; CRC Press: Boca Raton, FL, USA, 2007.
54. Imberdis, A.; Lefèvre, G.; Cantat, T. Transition-Metal-Free Acceptorless Decarbonylation of Formic Acid Enabled by a Liquid Chemical-Looping Strategy. *Angew. Chem. Int. Ed.* **2019**, *58*, 17215–17219. [[CrossRef](#)]
55. Wakizaka, M.; Matsumoto, T.; Tanaka, R.; Chang, H.-C. Dehydrogenation of Anhydrous Methanol at Room Temperature by O-Aminophenol-Based Photocatalysts. *Nat. Commun.* **2016**, *7*, 12333. [[CrossRef](#)]
56. Ruf, S.; May, A.; Emig, G. Anhydrous Formaldehyde by Sodium Catalysis. *Appl. Catal. A* **2001**, *213*, 203–215. [[CrossRef](#)]
57. Raich, B.A.; Foley, H.C. Ethanol Dehydrogenation with a Palladium Membrane Reactor: An Alternative to Wacker Chemistry. *Ind. Eng. Chem. Res.* **1998**, *37*, 3888–3895. [[CrossRef](#)]
58. Mooksuwan, W.; Kumar, S. Study on 2-Propanol/Acetone/Hydrogen Chemical Heat Pump: Endothermic Dehydrogenation of 2-Propanol. *Int. J. Energy Res.* **2000**, *24*, 1109–1122. [[CrossRef](#)]
59. Davis, J.L.; Barteau, M.A. Decarbonylation and Decomposition Pathways of Alcohol's on Pd(111). *Surf. Sci.* **1987**, *187*, 387–406. [[CrossRef](#)]
60. Olsen, E.P.K.; Singh, T.; Harris, P.; Andersson, P.G.; Madsen, R. Experimental and Theoretical Mechanistic Investigation of the Iridium-Catalyzed Dehydrogenative Decarbonylation of Primary Alcohols. *J. Am. Chem. Soc.* **2015**, *137*, 834–842. [[CrossRef](#)] [[PubMed](#)]
61. Orosz, K.; Papp, G.; Kathó, Á.; Joó, F.; Horváth, H. Strong Solvent Effects on Catalytic Transfer Hydrogenation of Ketones with [Ir(cod)(NHC)(PR<sub>3</sub>)] Catalysts in 2-Propanol-Water Mixtures. *Catalysts* **2020**, *10*, 17. [[CrossRef](#)]
62. Pavlova, A.; Meijer, E.J. Understanding the Role of Water in Aqueous Ruthenium-Catalyzed Transfer Hydrogenation of Ketones. *ChemPhysChem* **2012**, *13*, 3492–3496. [[CrossRef](#)] [[PubMed](#)]
63. Ambrose, D.; Sprake, C.H.S.; Townsend, R. Thermodynamic Properties of Organic Oxygen Compounds XXXVII. Vapour Pressures of Methanol, Ethanol, Pentan-1-ol, and Octan-1-ol from the Normal Boiling Temperature to the Critical Temperature. *J. Chem. Thermodyn.* **1975**, *7*, 185–190. [[CrossRef](#)]
64. Ruppert, A.M.; Jędrzejczyk, M.; Sneka-Platek, O.; Keller, N.; Dumon, A.S.; Michel, C.; Sautet, P.; Grams, J. Ru Catalysts for Levulinic Acid Hydrogenation with Formic Acid as a Hydrogen Source. *Green Chem.* **2016**, *18*, 2014–2028. [[CrossRef](#)]

**Publisher's Note:** MDPI stays neutral with regard to jurisdictional claims in published maps and institutional affiliations.



© 2020 by the authors. Licensee MDPI, Basel, Switzerland. This article is an open access article distributed under the terms and conditions of the Creative Commons Attribution (CC BY) license (<http://creativecommons.org/licenses/by/4.0/>).